Supplement of Atmos. Chem. Phys., 20, 5629–5644, 2020
https://doi.org/10.5194/acp-20-5629-2020-supplement

Atmospheric Chemistry and Physics
Open Access
EGU

Supplement of

Composition and volatility of secondary organic aerosol (SOA) formed from oxidation of real tree emissions compared to simplified volatile organic compound (VOC) systems

Arttu Ylisirniö et al.

Correspondence to: Arttu Ylisirniö (arttu.ylisirnio@uef.fi)

S1. Sesquiterpene mixture and Scots pine emission description

Table S1. Identified compounds and their relative contributions to the sesquiterpene mixture, based on GC-MS analysis.

Compound	Fraction %
cis-β-farnesene	7.89 ± 0.44
(E)-β-farnesene	9.56 ± 0.11
(Z.Z)-α-farnesene	8.47 ± 0.24
(E.Z)-α-farnesene	7.25 ± 0.08
cis-α-farnesene	6.69 ± 0.29
trans-α-bisabolene	5.46 ± 0.38
β-bisabolene	9.73 ± 0.19
trans-γ-bisabolene	4.51 ± 0.11
cis-α-bisabolene	18.31 ± 0.64
unidentified SQT	4.49 ± 0.10
unidentified SQT	3.98 ± 0.29
unidentified SQT	5.95 ± 0.13
unidentified SQT	7.73 ± 0.11

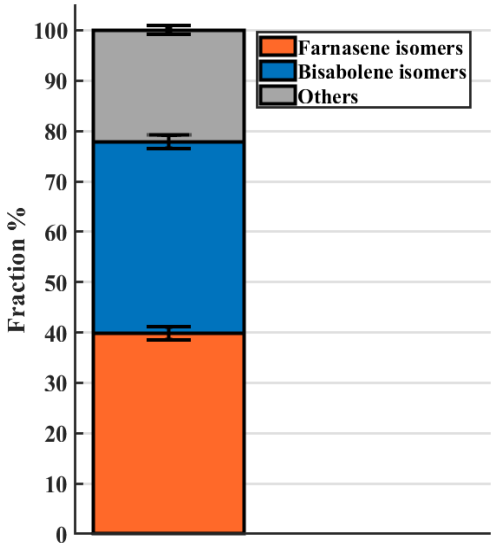

Figure S1: Graphical representation of data from Table S1, where different isomers of farnesene and bisabolene are summed up together. Unidentified compounds are summed into the "Others" class.

Table S2. Identified compounds and their relative contributions to the Scots pine emissions, based on GC-MS analysis.

Monoterpenes	**Fraction from total emission % (Scots pine exp. 1)**	**Fraction from total emission % (Scots pine exp. 4)**
β-phellandrene	13.11 ± 0.56	30.87 ± 12
3-carene	9.22 ± 0.8	15.42 ± 1.44
d-limonene	8.40 ± 0.87	12.68 ± 3.01
β-pinene	7.13 ± 0.42	7.98 ± 3.36
α-pinene	4.29 ± 0.17	6.99 ± 1.64
myrcene	1.17 ± 0.24	2.62 ± 0.34
terpinolene	1.15 ± 1.07	1.58 ± 1.32
camphene	0.61 ± 0.02	1.93 ± 0.3
o-cymene	0.47 ± 0.07	0.7 ± 0.13
α-phellandrene	0.43 ± 0.6	0.6 ± 0.27
ɣ-terpinene	0.21 ± 0.14	0.77 ± 0.36
cymenene	0.17 ± 0.06	0.36 ± 0.01
trans-β-ocimene	0.09 ± 0.05	0.1 ± 0.02
α-fenchene	0.05 ± 0.01	0.05 ± 0.01
sabinene	0.03 ± 0.01	0.06 ± 0.01
Sesquiterpenes	**Fraction from total emission % (Scots pine exp. 1)**	**Fraction from total emission % (Scots pine exp. 4)**
trans-β-farnesene	41.17 ± 0.58	14.3 ± 4.68
α-farnesene	9.81 ± 0.95	1.83 ± 0.73
α-bisabolene	2.13 ± 0.14	0.61 ± 0.14
aromadendrene	0.14 ± 0.07	0.09 ± 0.06
β-caryophyllene	0.06 ± 0.04	0.12 ± 0.07
α-humulene	0.06 ± 0.03	0.15 ± 0.04
α-copaene	0.06 ± 0.01	0.09 ± 0.01
β-elemene	0.03 ± 0.01	0.02 ± 0.01
longifolene	0.01 ± 0.01	0

10

S2. Experimental setup

SOA was generated by oxidizing different VOCs by OH radicals and O_3 in the OFR, in the absence of seed particles. VOCs were introduced by flushing clean air/N_2 through different sources. For the Scots pine experiments, VOCs were introduced by flushing purified air through a plant enclosure containing a 6-year-old Scots pine sapling. For α-pinene and sesquiterpenes SOA experiments, VOC vapors were introduced into a flow of dry N_2 using a diffusion source or a dynamic dilution system (Kari et al., 2018). In the dynamic dilution system, a set volume of VOCs was continuously injected into a heated N_2 flow with a syringe pump. The VOC-containing flow was then mixed with other make-up flows before entering the OFR. To achieve the desired RH, water vapor was introduced by passing a flow of N_2 through a Nafion humidifier (Model FC100-80-6MSS, Perma Pure). O_3 was generated in an external generator by irradiating a flow of O_2 or purified air with a 185-nm UV lamp. The exact ratios of these flows (humidified, VOC-, and O_3-contianing flows) varied between the different sets of experiments. But all relevant parameters of the mixture entering the OFR were carefully monitored and are given in Table 1 and 2. The mixing ratio of VOCs was continuously measured by a proton transfer reaction time-of-flight mass spectrometer (PTR-MS, PTR-TOF 8000, Ionicon Analytik, Austria) before mixing with O_3. To minimize line losses, the combined PFA (~2.5m, 6 mm outer diameter) and PEEK (~1 m, 1/16'' outer diameter) sampling line to the PRT-MS was heated to 60 °C. All other sampling lines were unheated stainless steel or conductive silicon tubing (Tygon®) as this work was focused on the particle phase composition. Overall, 2.5 or 5 L min^{-1} of mixed flow containing 200 - 400 ppb of VOCs was introduced into the OFR for photooxidation and ozonolysis, with leads to residence times in the OFR ranging from 120 to 300 s (assuming plug flow).

Inside the OFR, $O(^1D)$ was generated from the photolysis of O_3 with 254 nm lamps and reacted with water vapor to form OH radicals. To minimize the impact of heat generated from the 254-nm lamps, we continuously purged the lamps with N_2. We varied the OH exposure by adjusting the voltage of the 254-nm lamps inside the OFR and/or the ingoing O_3 concentration. The resulting OH exposure ranged from approx. 6.6×10^{10} to 2.5×10^{12} molec cm^{-3} s in the OFR, using the model calculations described by Peng et al. (2015, 2016) taking the external OH reactivity into account. Assuming an ambient OH concentration of 1.5×10^{6} molec cm^{-3}, this range of OH exposure corresponds to 0.5 to 19 equivalent days of atmospheric aging. Before and after each SOA experiment, we always conduced photooxidation cleaning for the OFR for several hours, i.e. flushing the PAM reactor with the same flows as during the experiments but without adding any VOCs. Background particle number concentration decreased to less than 2,000 # cm^{-3}, (particle mass < 0.1 µg m^{-3}. These values were neglectable in comparison to the 10^6 – 10^8 particles # cm^{-3} (and 50 – 500 µg m^{-3}) which were formed during the experiments. After the photooxidation cleaning, the VOC concentrations detected with the PTR-MS were within the instrument background. Care was taken to allow sufficient time after the VOC type or concentrations was changed.

S3. PTR-MS calibration

The PTR-MS was calibrated using a calibration gas standard with 8 aromatic compounds of mixing ratios ~100 ppbv in nitrogen (BOC, United Kingdom). The same gas standard was used to correct for non-ideal transmission in the instrument. Monoterpene and sesquiterpene concentrations were estimated from the Scots pine emission data using the ion signals of the protonated compounds at *m/z* 137 for monoterpenes and *m/z* 205 for sesquiterpenes, and accounting for the fragmentation of these ions by applying factors of 0.478 for monoterpenes and 0.5 for sesquiterpenes (compare Kari et. al., 2018).

S4. SOA characterisation

The outflow of the OFR was periodically checked with the PTR-MS to ensure that our assumption of complete consumption of the ingoing VOCs was correct. The same 2.5 m (outer diameter 6 mm) PFA + 1 m (outer diameter 1/16'') PEEK line heated to 60 °C was used for sampling before or after the OFR. When the sampling point was changed sampling lasted at least 30 min to ensure all compounds had reached their final values (especially sesquiterpenes).

The outflow of the OFR was continuously monitored with an AMS and a SMPS. The SMPS was operated with a closed loop sheath flow. The RH and temperature measured in the sheath flow in the instrument was close to the experimental conditions in the OFR.

The AMS was operated in V-mode and although particle size resolved data was collected, only the integrated signal was used for the analysis. The raw data was processed with the SQUIRREL (Version 1.59D) and PIKA toolkits (Version 1.19, Decarlo et al., 2006). As the composition of the "air" in OFR changed depending on the ratio between the N_2 and O_2 flows introduced into it, a time dependent air beam and CO_2 correction was applied. The main purpose of the AMS measurements were to classify the SOA particles by their oxidation state (O:C and H:C ratios, OS_C). The improved parameterisation from Canagaratna et al., 2015 was used to derive these values from the data.

S5. FIGAERO-CIMS calibration

The FIGAERO-CIMS mass axis was calibrated using known reagent ions and background signals, such as I^-, H_2OI^-, HNO_3I^-, I_2^-, I_3^-. Sensitivity calibration was not performed as each observed molecule should have been identified and calibrated individually, which was not possible with the experimental setup our study is based on. We therefore mostly show normalized data.

The conversion from peak desorption temperatures T_{max} to saturation vapor pressure P_{sat} and from there to saturation vapor concentration C^* was performed using a modified calibration method based on Bannan et al., 2019, using a series of polyethylene glycols (PEG) as reference compounds. Details of that modification will be published shortly in a separate publication. Calibration was done by fitting eq. S1 to measured values of T_{max} and literature-based values of P_{sat} for the PEGs:

$$P_{sat} = \exp(bT_{max} + a), \quad \text{(S1)}$$

where a and b are fitting coefficients. These coefficients were the following for FIGAERO inlets 1 and 2:

FIGAERO 1: a = -1.431, b = -0.207
FIGAERO 2: a = -3.929, b = -0.132.

P_{sat} was then converted to C^* with the assumptions of the ideal gas law.

S6. Extended discussion of SOA volatility

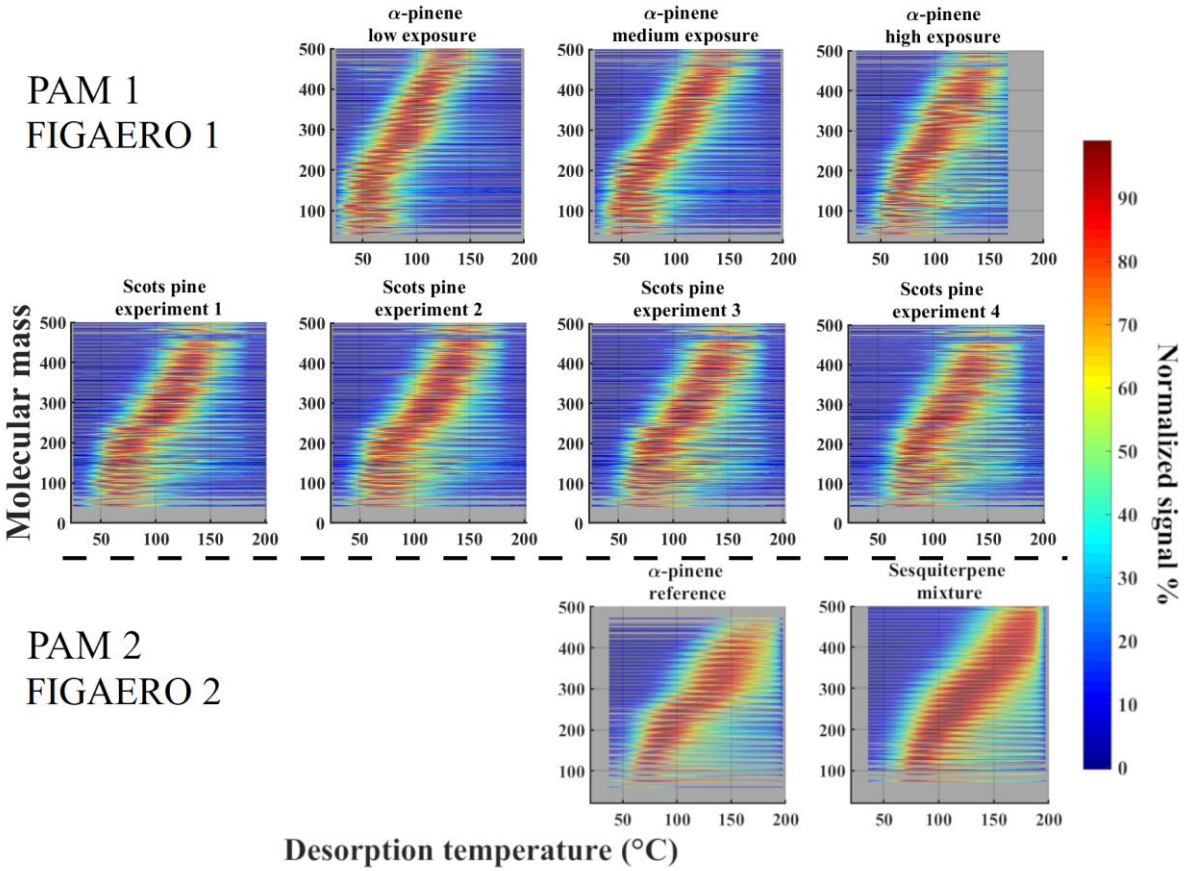

Figure S2: Individual ions' thermograms from each experiment, each depicted as a separate two-dimensional, coloured plot. The x-axes show desorption temperature; y-axes nominal (integer) ion mass. For clarity, signals have been summed up for each nominal mass, and colours show the intensity of said nominal mass normalized to the respective thermogram's maximum signal. Top row: α-pinene experiments (cf. Fig. 5a). Middle row: Scots pine experiments (cf. Fig. 5b). Bottom row: experiments using PAM 2 (sesquiterpene mixture and reference α-pinene experiment; cf. Fig. 5c).

Figure S2 reveals that the T_{max} values of detected ions are in general dependent on their molecular weight, as is expected. However, this dependence tends to disappear for ions corresponding to compounds with molecular weights less than around 150 Da, and their T_{max} tend to fall inside the same range. On the one hand, that is likely a form of observational bias, as at this lower molecular weight range, only lower-volatility compounds would partition into the particle phase. On the other hand, as mentioned above, we can expect at least some compounds with lower molecular weights to be products of thermal decomposition of larger compounds. More apparent signatures of thermal decomposition are visible as well: thermograms peaking at clearly higher temperatures than expected by the respective molecular weight, and thermograms substantially

extending towards higher temperatures (tailing). Both of those signatures have also been extensively observed also in previous studies (Wang et al., 2016, D'Ambro et al., 2017; Lopez-Hilfiker et al., 2014; Lopez-Hilfiker et al., 2015; Lopez-Hilfiker et al., 2016; Schobesberger et al., 2018).

The top row of Fig. S2 shows that not only do the sum thermograms for the α-pinene experiments shift to higher desorption temperatures with increasing oxidation exposure, but the shift is essentially seen throughout the spectrum of individual thermograms (cf. Fig. 5). In addition, an increasing role of thermal decomposition is apparent, especially through increasing tailing of the thermograms. In the same manner, T_{max} values are increased throughout the spectrum when comparing the reference α-pinene to the sesquiterpene mixture experiment (bottom row Fig. S2), with notable contributions of decomposition processes in both cases. In line with these observations, and those in Figs. 4-5, the plots obtained from the Scots pine experiments (middle row Fig. S2) broadly appear as expected: as in-between cases between the α-pinene and the sesquiterpene results. As in Fig. 5, Scots pine experiment 4 features the highest T_{max} values, and also somewhat larger apparent contributions by thermal decomposition products. But overall, the similarities to the other Scots pine experiments (especially experiment 3) predominate (cf. Fig. 4), in spite of the much higher contribution of monoterpenes than in experiments 1-3.

References:

Bannan, T. J., Le Breton, M., Priestley, M., Worrall, S. D., Bacak, A., Marsden, N. A., Mehra, A., Hammes, J., Hallquist, M., Alfarra, M. R., Krieger, U. K., Reid, J. P., Jayne, J., Robinson, W., McFiggans, G., Coe, H., Percival, C. J. and Topping, D.: A method for extracting calibrated volatility information from the FIGAERO-HR-ToF-CIMS and its experimental application, Atmos. Meas. Tech., 12(3), 1429–1439, doi:10.5194/amt-12-1429-2019, 2019.

Canagaratna, M. R., Jimenez, J. L., Kroll, J. H., Chen, Q., Kessler, S. H., Massoli, P., Hildebrandt Ruiz, L., Fortner, E., Williams, L. R., Wilson, K. R., Surratt, J. D., Donahue, N. M., Jayne, J. T. and Worsnop, D. R.: Elemental ratio measurements of organic compounds using aerosol mass spectrometry: Characterization, improved calibration, and implications, Atmos. Chem. Phys., 15(1), 253–272, doi:10.5194/acp-15-253-2015, 2015.

D'Ambro, E. L., Lee, B. H., Liu, J., Shilling, J. E., Gaston, C. J., Lopez-Hilfiker, F. D., Schobesberger, S., Zaveri, R. A., Mohr, C., Lutz, A., Zhang, Z., Gold, A., Surratt, J. D., Rivera-Rios, J. C., Keutsch, F. N. and Thornton, J. A.: Molecular composition and volatility of isoprene photochemical oxidation secondary organic aerosol under low- and high-NOx conditions, Atmos. Chem. Phys., 17(1), 159–174, doi:10.5194/acp-17-159-2017, 2017.

DeCarlo, P. F., Kimmel, J. R., Trimborn, A., Northway, M. J., Jayne, J. T., Aiken, A. C., Gonin, M., Fuhrer, K., Horvath, T., Docherty, K. S., Worsnop, D. R. and Jimenez, J. L.: Field-deployable, high-resolution, time-of-flight aerosol mass spectrometer, Anal. Chem., 78(24), 8281–8289, doi:10.1021/ac061249n, 2006.

Kari, E., Miettinen, P., Yli-Pirilä, P., Virtanen, A. and Faiola, C. L.: PTR-ToF-MS product ion distributions and humidity-

dependence of biogenic volatile organic compounds, Int. J. Mass Spectrom., 430, 87–97, doi:10.1016/j.ijms.2018.05.003, 2018.

Lopez-Hilfiker, F. D., Mohr, C., Ehn, M., Rubach, F., Kleist, E., Wildt, J., Mentel, T. F., Lutz, A., Hallquist, M., Worsnop, D. and Thornton, J. A.: A novel method for online analysis of gas and particle composition: Description and evaluation of a filter inlet for gases and AEROsols (FIGAERO), Atmos. Meas. Tech., 7(4), 983–1001, doi:10.5194/amt-7-983-2014, 2014.

Lopez-Hilfiker, F. D., Mohr, C., Ehn, M., Rubach, F., Kleist, E., Wildt, J., Mentel, T. F., Carrasquillo, A. J., Daumit, K. E., Hunter, J. F., Kroll, J. H., Worsnop, D. R. and Thornton, J. A.: Phase partitioning and volatility of secondary organic aerosol components formed from α-pinene ozonolysis and OH oxidation: The importance of accretion products and other low volatility compounds, Atmos. Chem. Phys., 15(14), 7765–7776, doi:10.5194/acp-15-7765-2015, 2015.

Lopez-Hilfiker, F. D., Iyer, S., Mohr, C., Lee, B. H., D'ambro, E. L., Kurtén, T. and Thornton, J. A.: Constraining the sensitivity of iodide adduct chemical ionization mass spectrometry to multifunctional organic molecules using the collision limit and thermodynamic stability of iodide ion adducts, Atmos. Meas. Tech., 9(4), 1505–1512, doi:10.5194/amt-9-1505-2016, 2016.

Schobesberger, S., D'Ambro, E. L., Lopez-Hilfiker, F. D., Mohr, C. and Thornton, J. A.: A model framework to retrieve thermodynamic and kinetic properties of organic aerosol from composition-resolved thermal desorption measurements, Atmos. Chem. Phys., 18(20), 14757–14785, doi:10.5194/acp-18-14757-2018, 2018.

Wang, M., Yao, L., Zheng, J., Wang, X., Chen, J., Yang, X., Worsnop, D. R., Donahue, N. M. and Wang, L.: Reactions of Atmospheric Particulate Stabilized Criegee Intermediates Lead to High-Molecular-Weight Aerosol Components, Environ. Sci. Technol., 50(11), 5702–5710, doi:10.1021/acs.est.6b02114, 2016.